# BRAIN
A JOURNAL OF NEUROLOGY

# *In vivo* radioligand binding to translocator protein correlates with severity of Alzheimer's disease

William C. Kreisl,[1] Chul Hyoung Lyoo,[1] Meghan McGwier,[1] Joseph Snow,[2] Kimberly J. Jenko,[1] Nobuyo Kimura,[1] Winston Corona,[3] Cheryl L. Morse,[1] Sami S. Zoghbi,[1] Victor W. Pike,[1] Francis J. McMahon,[3] R. Scott Turner,[4] Robert B. Innis[1] and the Biomarkers Consortium PET Radioligand Project Team

1 Molecular Imaging Branch, National Institute of Mental Health, Bethesda, MD, USA
2 Office of the Clinical Director, National Institute of Mental Health, Bethesda, MD, USA
3 Human Genetics Branch, National Institute of Mental Health, Bethesda, MD, USA
4 Memory Disorders Program, Georgetown University, Washington, DC, USA

Correspondence to: William C. Kreisl, MD
National Institute of Mental Health,
10 Center Drive, Rm. B1/D43,
Bethesda, MD,
20892-1026, USA
E-mail: kreislw@mail.nih.gov

Neuroinflammation is a pathological hallmark of Alzheimer's disease, but its role in cognitive impairment and its course of development during the disease are largely unknown. To address these unknowns, we used positron emission tomography with $^{11}$C-PBR28 to measure translocator protein 18 kDa (TSPO), a putative biomarker for inflammation. Patients with Alzheimer's disease, patients with mild cognitive impairment and older control subjects were also scanned with $^{11}$C-Pittsburgh Compound B to measure amyloid burden. Twenty-nine amyloid-positive patients (19 Alzheimer's, 10 mild cognitive impairment) and 13 amyloid-negative control subjects were studied. The primary goal of this study was to determine whether TSPO binding is elevated in patients with Alzheimer's disease, and the secondary goal was to determine whether TSPO binding correlates with neuropsychological measures, grey matter volume, $^{11}$C-Pittsburgh Compound B binding, or age of onset. Patients with Alzheimer's disease, but not those with mild cognitive impairment, had greater $^{11}$C-PBR28 binding in cortical brain regions than controls. The largest differences were seen in the parietal and temporal cortices, with no difference in subcortical regions or cerebellum. $^{11}$C-PBR28 binding inversely correlated with performance on Folstein Mini-Mental State Examination, Clinical Dementia Rating Scale Sum of Boxes, Logical Memory Immediate (Wechsler Memory Scale Third Edition), Trail Making part B and Block Design (Wechsler Adult Intelligence Scale Third Edition) tasks, with the largest correlations observed in the inferior parietal lobule. $^{11}$C-PBR28 binding also inversely correlated with grey matter volume. Early-onset (<65 years) patients had greater $^{11}$C-PBR28 binding than late-onset patients, and in parietal cortex and striatum $^{11}$C-PBR28 binding correlated with lower age of onset. Partial volume corrected and uncorrected results were generally in agreement; however, the correlation between $^{11}$C-PBR28 and $^{11}$C-Pittsburgh Compound B binding was seen only after partial volume correction. The results suggest that neuroinflammation, indicated by increased $^{11}$C-PBR28 binding to TSPO, occurs after conversion of mild cognitive impairment to Alzheimer's disease and worsens with disease progression. Greater inflammation may contribute to the precipitous disease course typically seen in early-onset patients. $^{11}$C-PBR28 may be useful in longitudinal studies to mark the conversion from mild cognitive impairment or to assess response to experimental treatments of Alzheimer's disease.

# Introduction

Neuroinflammation, consisting of microglial activation and/or reactive astrocytosis, has long been considered a potential contributor to pathogenesis in Alzheimer's disease (McGeer and McGeer, 2003). However, the exact role and timing of neuroinflammation in Alzheimer's disease is controversial, as inflammatory brain changes have been reported in both early and late stages of the disease (Craft et al., 2006; Xiang et al., 2006; Eikelenboom et al., 2010). In addition, results from some studies suggest microglial activation is actually neuroprotective against Alzheimer's disease (El Khoury et al., 2007) and that Alzheimer's disease neuropathology is associated with senescent, rather than activated, microglia (Streit et al., 2009). Patients with mild cognitive impairment (MCI) are at increased risk for progression to Alzheimer's disease, and patients with MCI with amyloid pathology—as identified through PET using ^{11}C-Pittsburgh Compound B (PIB)—convert to Alzheimer's disease at reported rates as high as 48% within 3 years (Okello et al., 2009b; Wolk et al., 2009). Therefore PIB-positive patients with MCI likely represent a prodromal stage of Alzheimer's disease, and studying inflammation in these patients may shed light on whether microglial activation is an early contributor to Alzheimer's disease pathogenesis.

PET imaging allows in vivo quantification of neuroinflammation by measuring the density of the 18 kDa translocator protein (TSPO). TSPO is a mitochondrial protein expressed by immune competent cells in the brain (microglia and astrocytes) and in the periphery (Papadopoulos et al., 2006). When activated through host response to cellular injury, microglia and astrocytes over-express TSPO. [11]C-(R)-PK 11195, the prototypical TSPO radioligand, has been used to measure neuroinflammatory changes in several diseases, including Alzheimer's disease (Cagnin et al., 2001) and [11]C-(R)-PK 11195 binding has been shown to correlate with Mini-Mental State Examination score in patients with Alzheimer's disease (Edison et al., 2008). However, there have been conflicting reports about whether [11]C-(R)-PK 11195 binding is increased in Alzheimer's disease or not (Cagnin et al., 2001; Wiley et al., 2009; Schuitemaker et al., 2013). Whether [11]C-(R)-PK 11195 binding is increased in MCI appears even less conclusive. For instance, Okello and colleagues (2009a) found a small increase in [11]C-(R)-PK 11195 in PIB-positive patients with MCI relative to controls, but other studies found no increase in patients with MCI, even those who later progressed to dementia (Wiley et al., 2009; Schuitemaker et al., 2013).

Several second generation TSPO radioligands have been developed (Chauveau et al., 2008). Of these, only ^{11}C-DAA1106 has been used to detect increased TSPO in Alzheimer's disease (Yasuno et al., 2008). In that study, patients with Alzheimer's disease had greater ^{11}C-DAA1106 binding than control subjects in several brain regions, including regions typically less affected by the disease, such as cerebellum and occipital cortex. That study found no correlation between ^{11}C-DAA1106 binding and disease severity. However, ^{11}C-DAA1106 has slow washout of brain relative to the short half-life of [11]C (Ikoma et al., 2007), which could confound accurate estimation of binding values (Imaizumi et al., 2007).

[11]C-PBR28 is a second generation radioligand with high affinity to TSPO, favourable in vivo kinetics, and greater signal-to-noise ratio than [11]C-(R)-PK 11195 in monkey brain (Fujita et al., 2008; Kreisl et al., 2010). No similar direct comparison of these two radioligands has been reported in humans; thus, we do not know whether the results in monkeys accurately reflect that in humans. The main limitation of ^{11}C-PBR28, shared by all tested second generation TSPO radioligands (including ^{11}C-DAA1106), is differential affinity for the target protein (Owen et al., 2011). This differential affinity is caused by the rs6971 polymorphism on the TSPO gene that causes a non-conservative amino acid substitution, resulting in three patterns of TSPO binding (Owen et al., 2012). Subjects without the polymorphism (HH) have high affinity binding for PBR28, homozygotes (LL) have low affinity binding, and heterozygotes (HL) express both high and low affinity TSPO (mixed-affinity binding). Low affinity subjects are easily identified by PET due to negligible ^{11}C-PBR28 binding in vivo; however, PET cannot easily resolve the difference between high and mixed-affinity subjects, and mixed-affinity subjects have, on average, 22% less total ^{11}C-PBR28 binding than high affinity subjects (Kreisl et al., 2013). Previous work from our laboratory demonstrated that correcting in vitro binding data for rs6971 genotype improves the ability of ^{3}H-PBR28 to detect differences in TSPO density in schizophrenia and control brain tissue (Kreisl et al., 2013). This strategy of TSPO genotype correction to PET imaging was used in the present study, which sought to determine whether Alzheimer's disease is associated with increased ^{11}C-PBR28 binding in vivo.

Specifically, we investigated the relationship between neuroinflammation and disease severity in Alzheimer's disease by performing ^{11}C-PBR28 PET in patients with Alzheimer's disease and MCI, and in age-matched control subjects. We also looked for correlative relationships between ^{11}C-PBR28 binding and clinical severity, grey matter volume loss and amyloid burden. Finally, we compared ^{11}C-PBR28 binding in early- and late-onset patients to determine whether early disease onset was associated with greater inflammation.

# Materials and methods

## Subject selection

Patients and healthy controls were recruited by the Molecular Imaging Branch of the National Institute of Mental Health (NIMH). The study was approved by the National Institutes of Health (NIH) Combined Neurosciences Institutional Review Board, and all participants or their surrogate signed informed consent before entering the study. All

subjects underwent an extensive medical and neurological workup. All subjects had brain MRIs, and nine patients underwent ^{18}F-fluorodeoxyglucose PET as part of the evaluation. Subjects with significant co-morbid medical or psychiatric illness were excluded from the study, as were those with significant cerebrovascular disease (defined as severe white matter hyperintensities found on MRI). Diagnosis was based on the consensus of two neurologists or one neurologist and one neuro-psychologist. All patients with Alzheimer's disease who underwent ^{11}C-PBR28 imaging met National Institute of Neurological and Communicative Disorders and Stroke-Alzheimer's Disease and Related Disorders Association (NINCDS-ADRDA) criteria for probable Alzheimer's disease (McKhann *et al.*, 1984) and updated criteria for probable Alzheimer's disease dementia with evidence of the Alzheimer's disease pathophysiological process (McKhann *et al.*, 2011). All patients with MCI who underwent ^{11}C-PBR28 imaging met Petersen criteria for MCI (Petersen, 2004) and updated criteria for MCI due to Alzheimer's disease of high or intermediate likelihood (Albert *et al.*, 2011). All patients with Alzheimer's disease and MCI presented with a memory complaint. Whereas some patients with Alzheimer's disease had impairment of non-memory domains on testing, all had memory involvement. No patient had early language involvement out of proportion to memory impairment suggestive of logopenic progressive aphasia. It is important to note that only 'PIB-positive' Alzheimer's disease and patients with MCI, and 'PIB-negative' controls, had ^{11}C-PBR28 imaging. To compare ^{11}C-PBR28 binding in early- and late-onset patients, symptom onset was determined according to history from patient and informants. Onset age <65 years was defined as early-onset.

## Neuropsychological assessment

The neuropsychological testing battery was adapted from the Uniform Data Set to be consistent with batteries used in previous studies that stratify patients into MCI and Alzheimer's disease cohorts (Weintraub *et al.*, 2009). These tests included: the Folstein Mini-Mental State Examination; Clinical Dementia Rating Scale; Wechsler Test of Adult Reading; Digit-Symbol, Block Design, and Similarities tests from the Wechsler Adult Intelligence Scale Third Edition; the Trail Making Test, Parts A and B; the Wechsler Memory Scale Third Edition; the Hopkins Verbal Learning Test Revised; the Brief Visual Memory Test Revised; the Wisconsin Card Sorting Test, 64-item (WCST-64); the Benton Visual Form Discrimination Test; the Boston Naming Test; the Controlled Oral Word Association Test for letter (FAS) and category (animals) fluency; the Grooved Pegboard Test (dominant and non-dominant hands); the Beck Depression Inventory; and the Beck Anxiety Inventory. Three patients (all with Alzheimer's disease) had only partial neuropsychological data available, but this included at least the Folstein Mini-Mental State Examination, Clinical Dementia Rating Scale, Wechsler Memory Scale or Brief Visual Memory Test, Trail Making Test, Boston Naming Test, and letter and category fluency tests.

## Brain magnetic resonance imaging

To determine anatomical boundaries for volumetric analysis and partial volume correction, high-resolution sagittal $T_1$-weighted magnetic resonance images were acquired in a 3 T Philips Achieva scanner using turbo field echo sequence (repetition time = 8.1 ms, echo time = 3.7 ms, flip angle = 8°, matrix = 181 × 256 × 256, voxel size = 1 × 0.983 × 0.983 mm). Magnetic resonance images and ^{11}C-PBR28 images were acquired within 1 year of each other for each subject.

## PBR28 positron emission tomography imaging

[11]C-PBR28 was synthesized as described in Investigational New Drug Application #76 441, a copy of which is available at: http://pdsp.med.unc.edu/snidd/. At injection, ^{11}C-PBR28 had high radiochemical purity (>99%) and specific activity of 138 ± 67 GBq/μmol (Alzheimer's disease: 135 ± 80 GBq/μmol; MCI: 152 ± 54 GBq/μmol; healthy control subjects: 133 ± 59 GBq/μmol). The injected dose of ^{11}C-PBR28 was 673 ± 40 MBq (Alzheimer's disease: 684 ± 15 MBq; MCI: 683 ± 15 MBq; healthy control subjects: 651 ± 64 MBq).

Arterial blood was manually sampled at 15-s intervals for the first 2 min 30 s, then at 3, 4, 6, 8, 10, 15, 20, 30, 40, 50, 60, 75, and 90 min. Radioactivity in plasma was quantified by a gamma-counter and analysed by reverse-phase chromatography to separate parent radioligand from radiometabolites (Zoghbi *et al.*, 2006). Free fraction of ^{11}C-PBR28 in plasma ($f_P$) was measured by ultrafiltration and normalized using a standard derived from pooled donor plasma (Abi-Dargham *et al.*, 1995).

## Pittsburgh compound B positron emission tomography imaging

PIB was synthesized as previously reported (Klunk *et al.*, 2004). Synthesis was performed in accordance with Investigational New Drug Application #108,861. PIB was synthesized with high radiochemical purity (>99%) and had specific activity at the time of injection of 88 ± 55 GBq/μmol (Alzheimer's disease: 99 ± 57 GBq/μmol; MCI: 81 ± 35 GBq/μmol; healthy control subjects: 79 ± 65 GBq/μmol).

An 8 min [68]Ge transmission scan was performed for attenuation correction, and PIB was then injected as an intravenous bolus. The injected dose of radioactivity from PIB administration was 366 ± 12 MBq (Alzheimer's disease: 366 ± 14 MBq; MCI: 368 ± 6 MBq; healthy control subjects: 364 ± 12 MBq). The PET scan was acquired in 3D dynamic mode using a GE Advance tomograph (GE Medical Systems) with frame duration of 15 s × 4, 30 s × 8, 1 min × 9, 3 min × 2, 5 min × 8, and 10 min × 1, for a total scan time of 70 min.

## Image analysis

### General approach

Our general approach to image analysis sought to reflect two aspects of the neuropathology of Alzheimer's disease. First, because the primary pathology of Alzheimer's disease is in grey rather than white matter, we analysed MRI and PET images so as to preferentially measure radioactivity in grey matter. Such approaches have been used in Alzheimer's disease to measure amyloid burden in the Alzheimer's Disease Neuroimaging Initiative (Landau *et al.*, 2013) and in other dementias with preferential pathology in grey matter (Petrou *et al.*, 2012). Second, because grey matter is atrophied in Alzheimer's disease, the PET signal from grey matter is more diluted in Alzheimer's disease than in control subjects by adjacent areas of low (white matter) or negligible (CSF) radioactivity. Several methods of partial volume correction can compensate for atrophy and have been used in several disorders (Thomas *et al.*, 2011). However, because partial volume correction may artificially create a positive finding, we report the analysis of PET images both with and without partial volume correction.

To preferentially sample grey matter voxels, we first identified those voxels in the MRI with the greatest contribution from grey matter and then used these voxels to sample from the co-registered PET. FreeSurfer 5.1 (Massachusetts General Hospital, Harvard Medical School; http://surfer.nmr.mgh.harvard.edu) was used to obtain regional mask images of brain regions. Individual magnetic resonance images underwent transformation into 1 mm of isovoxel space, correction for inhomogeneity of signal intensity, skull-stripping, and segmentation into grey and white matter according to the intensity gradient and connectivity of voxels. Minimal manual correction was applied to correct misclassified tissues. By inflating the boundary between grey and white matter and overlaying curvature information on the inflated surface, cerebral cortex was parcellated with a probabilistic labelling algorithm (Fischl et al., 2004; Desikan et al., 2006). Non-cortical grey matter structures were segmented and labelled using probabilistic registration techniques (Fischl et al., 2002). By putting the regional information of parcellation on each voxel in the segmented image, a mask image containing 112 regional identifiers was reconstructed. Finally, 15 regions of interest were grouped for analysis, including target regions expected to have pathological changes related to Alzheimer's disease and background regions expected to be relatively spared. Target regions included prefrontal cortex (superior, middle, inferior, orbitofrontal), sensorimotor (precentral, paracentral, postcentral), inferior parietal lobule, precuneus, occipital cortex (medial, lateral, lingual), superior temporal cortex, middle and inferior temporal cortex, hippocampus, entorhinal cortex, parahippocampal gyrus, anterior cingulate cortex, and posterior cingulate cortex. Background regions included striatum (caudate and putamen), thalamus and cerebellar cortex. A composite white matter volume was also created. Regional cerebral volume was measured by counting the number of voxels in each region.

### ^{11}C-PBR28 image analysis

After correction for attenuation and scatter, PET images were reconstructed with filtered back projection algorithm in a $128 \times 128 \times 35$ matrix with a $2 \times 2 \times 4.25$ mm voxel size. Statistical parametric mapping 8 (SPM8; Wellcome Department of Cognitive Neurology, London, UK) implemented in MATLAB 7.1 (MathWorks) and PMOD version 3.17 (PMOD Technologies Ltd.) were used for preprocessing and kinetic analysis of PET images.

Reconstructed PET images were realigned for motion correction and coregistered to the $T_1$-weighted magnetic resonance image in 1 mm isovoxel space. Using binary mask images for all regions, we corrected partial volume effects of each PET image time frame with region-based voxel-wise correction technique programmed in MATLAB (Thomas et al., 2011). A 3D Gaussian kernel with 7 mm full-width at half-maximum was used as a point-spread function correcting the spill-in and spill-over.

For ^{11}C-PBR28 PET image analysis, we measured the time activity curve of each region before and after correction for partial volume effect. Metabolite corrected plasma and whole blood input function was fitted to tri-exponential function. Time delay between the radial artery and brain was calculated from the volume-weighted average time activity curve of all grey matter regions. With parent input functions and time activity curves, total distribution volume ($V_T$) and rate constants ($K_1$, $k_2$, $k_3$ and $k_4$) of the two tissue-compartmental model were calculated for each brain region as previously described (Fujita et al., 2008). We followed the proposed consensus nomenclature for reversibly binding radioligands (Innis et al., 2007), where $V_T$ is the sum of both specific and non-displaceable uptake. $V_T$ equals the ratio at equilibrium of the concentration of radioligand in brain to that in plasma and is proportional to receptor density.

### Pittsburgh compound B image analysis

PIB PET data were analysed using two different methods. The first method was adapted from Jack et al. (2008) and used to stratify subjects as PIB-positive or PIB-negative in order to include only subjects with amyloid pathology into the patient groups, and to exclude age-matched controls with incidental amyloid plaque deposition (see Supplementary material).

The second method was used to quantify the cortical amyloid plaque burden for correlative analysis with the PBR28 data. For this analysis of PIB PET images, we used time frames of PET images between 35 to 60 min and made both partial volume-corrected and uncorrected 4D PET images. Using the Logan reference tissue model with cerebellum as a reference tissue and $k_2' = 0.149$/min, distribution volume ratio images were generated (Price et al., 2005) and used to measure distribution volume ratio values within each region.

## TSPO genotype

Blood samples for genetic analysis were available for only 29 subjects (10 Alzheimer's disease, seven MCI, 12 control subjects), because the report that the rs6971 TSPO polymorphism responsible for differential affinity for PBR28 was not published (Owen et al., 2012) until several subjects had already completed study procedures. For these 29 subjects, genomic DNA was used to genotype the rs6971 polymorphism within the TSPO gene on chromosome 22q13.2, as previously described (Kreisl et al., 2013; Supplementary material).

We recently reported that in vitro receptor binding to TSPO on leucocyte membranes has 100% agreement with genotype (Kreisl et al., 2013) and were able to use this method to determine the genotype of early subjects without samples of DNA. The in vitro receptor binding method is described in the Supplementary methods.

## Statistical analysis

Statistical analysis was performed using SPSS Statistics 17.0. Differences in distribution volume corrected for free fraction of radioligand in plasma ($V_T / f_P$) of ^{11}C-PBR28 were compared among diagnostic groups using factorial ANOVA with TSPO genotype (number of H alleles) as a fixed factor and age and years of education as covariates. To directly compare ^{11}C-PBR28 binding within each genotype group, we stratified subjects by affinity status and ran a separate ANOVA. We performed this separate analysis for one representative target region (inferior parietal cortex) and one representative background region (cerebellum). Data from Alzheimer's disease and MCI groups were combined to look for associations between ^{11}C-PBR28 binding and clinical severity (raw scores on Mini-Mental State Examination, Logical Memory Immediate of the Wechsler Memory Scale Third Edition, Block Design of Wechsler Adult Intelligence Scale Third Edition, Trail Making part B, Wisconsin Card Sort Test Total Errors, and Clinical Dementia Rating Scale Sum of Boxes score), brain atrophy (grey matter voxel count), and amyloid burden (PIB distribution volume ratio values) using linear correlation analysis. These cognitive tests were selected because most patients had them performed and there was a dynamic range of results that were normally distributed. For correlation with neuropsychological measures, we examined regions affected by Alzheimer's disease with functional relationships to these measures, namely prefrontal cortex, inferior parietal lobule, middle and inferior temporal cortex, precuneus, and

entorhinal cortex. To correct for the effect of genotype, as well as age and education, correlations were first run between the individual outcome measures and genotype (with age and education as additional independent variables). Standardized residuals were then plotted against each other. Differences in ^{11}C-PBR28 binding between high and mixed-affinity groups were determined using factorial ANOVA with Mini-Mental State Examination score as a covariate to correct for differences in PBR28 binding associated with Alzheimer's disease pathology. Differences in ^{11}C-PBR28 binding between high and mixed affinity subjects within each diagnostic group were also determined using factorial ANOVA with age and education as covariates.

Data are given as mean ± SD.

# Results

## Demographic differences

Nineteen patients with Alzheimer's disease, 10 patients with MCI, and 13 controls completed all study procedures (Table 1). Diagnostic groups did not differ with regard to sex, education, or use of non-steroidal anti-inflammatory drugs ($P > 0.322$). Patients with MCI were on average 9 years older than patients with Alzheimer's disease and controls ($P = 0.012$). No difference in age was seen between patients with Alzheimer's disease and controls ($P = 0.998$). Duration of symptoms was the same between groups when patients were stratified based on MCI versus Alzheimer's disease ($P = 0.193$) and early- versus late-onset ($P = 0.232$). Patients had greater Clinical Dementia Rating Sum of Boxes scores than controls ($P < 0.02$) and patients with Alzheimer's disease had greater Clinical Dementia Rating Sum of Boxes and lower Mini-Mental State Examination scores than patients with MCI and controls ($P < 0.001$). Cholinesterase inhibitor use was more prevalent in patients with Alzheimer's disease than patients with MCI (79% versus 40%, $P = 0.036$).

Leucocyte binding results agreed with genotype results (one-site fit = HH; two-site fit = HL) in all 29 subjects who had both analyses performed. Therefore, for the remainder of the analysis, all subjects with one-site fit ($n = 18$) were considered high affinity and subjects with two-site fit ($n = 24$) were considered mixed-

affinity. Prevalence of mixed-affinity subjects was: 52.6% for Alzheimer's disease, 60.0% for MCI, and 61.5% for controls. All high affinity subjects (controls and patients combined) had greater ^{11}C-PBR28 binding than mixed-affinity subjects in a composite (whole brain) grey matter volume ($P < 0.001$), after correction for Mini-Mental State Examination score. In addition, for each diagnostic group, high affinity subjects had greater ^{11}C-PBR28 binding in whole brain than mixed-affinity subjects ($P < 0.03$).

As expected, both patients with Alzheimer's disease and patients with MCI had greater PIB binding (distribution volume ratio, uncorrected for partial volume effect) than controls, most notably in prefrontal, sensorimotor, lateral temporal, and cingulate cortex; parahippocampal gyrus; inferior parietal lobule; precuneus; and striatum ($P < 0.001$), with no difference in cerebellum ($P > 0.71$). Both patients with Alzheimer's disease and patients with MCI had greater hippocampal atrophy on MRI than controls (summed grey matter voxel count for right and left hippocampi: $6.63 \pm 0.98$ and $6.87 \pm 0.96$ versus $8.36 \pm 0.73$ cm$^3$, $P < 0.002$).

## ^{11}C-PBR28 binding and clinical severity

To determine the relationship between neuroinflammation and clinical severity in Alzheimer's disease, we first compared ^{11}C-PBR28 binding in patients with Alzheimer's disease, patients with MCI, and controls. In the partial volume corrected images, brain uptake of radioligand was greater in patients with Alzheimer's disease than in patients with MCI or controls in cortical regions known to be affected by Alzheimer's disease pathology (Fig. 1). Univariate ANOVA showed significant differences in ^{11}C-PBR28 binding among patients with Alzheimer's disease and patients with MCI and controls for all cortical regions except the anterior cingulate gyrus ($P < 0.05$, Table 2). Pairwise comparison showed that patients with Alzheimer's disease had greater binding than either patients with MCI or controls. Differences were greatest in inferior parietal lobule, middle and inferior temporal cortex, and precuneus ($P < 0.005$, Alzheimer's disease versus controls). No difference in ^{11}C-PBR28 binding was seen in white matter, thalamus, striatum or cerebellum. No difference in binding was

## Table 1 Demographic characteristics of study participants

| | Alzheimer's disease | MCI | Healthy control subjects |
|---|---|---|---|
| *n* | 19 | 10 | 13 |
| Age (years) | $63.1 \pm 8.8$ | $72.6 \pm 9.7$* | $62.9 \pm 6.4$ |
| Sex | 8 F, 11 M | 4 F, 6 M | 4 F, 9 M |
| Education (years) | $17.2 \pm 2$ | $16.4 \pm 2.6$ | $15.9 \pm 2.6$ |
| Duration (years) | $3.5 \pm 1.4$ | $2.8 \pm 1.3$ | N/A |
| Mini-Mental State Examination | $20.3 \pm 4.2$** | $27.5 \pm 2$ | $29.8 \pm 0.4$ |
| Clinical Dementia Rating Scale Sum of Boxes | $5.1 \pm 2.5$** | $2.2 \pm 1.0$† | $0 \pm 0$ |
| Genotype, HH:HL | 9:10 | 4:6 | 5:8 |
| $f_P$ | $0.039 \pm 0.006$ | $0.044 \pm 0.0072$ | $0.048 \pm 0.017$ |
| Non-steroidal anti-inflammatory drug use | 0.316 | 0.6 | 0.462 |
| Cholinesterase inhibitor | 78.9%$^{††}$ | 0.4 | 0 |

HH = high affinity binder; HL = mixed affinity binder; $f_P$ = plasma free fraction of ^{11}C-PBR28.
*$P < 0.03$ versus Alzheimers disease and healthy control subjects; **$P < 0.001$ versus MCI and healthy control subjects; †$P = 0.013$ versus healthy control subjects; $^{††}P = 0.036$ versus MCI.
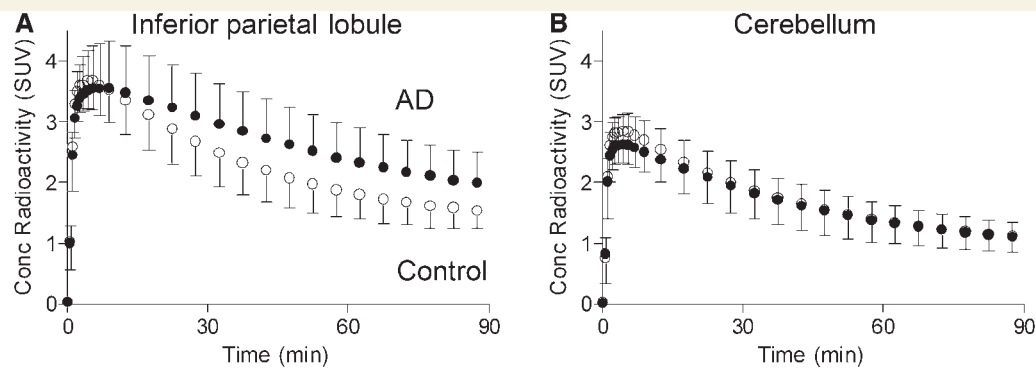
**Figure 1** Alzheimer's disease (AD) patients (filled circle) had greater uptake of $^{11}$C-PBR28 than healthy controls (open circle) in target, but not background, brain regions. Concentration of radioactivity after injection of $^{11}$C-PBR28, given as standardized uptake value (SUV) and corrected for partial volume effect, for inferior parietal lobule (**A**) and cerebellum (**B**) are shown. SUV = (concentration of activity per g tissue / injected activity) × g body weight. Data not adjusted for *TSPO* genotype. Data given as mean ± SD.

**Table 2** Regional $^{11}$C-PBR28 binding in Alzheimer's disease, MCI and healthy control subjects

|  | Alzheimer's disease, *n* = 19 | MCI, *n* = 10 | Healthy control subjects, *n* = 13 |
|---|---|---|---|
| Region |  |  |  |
| Prefrontal | 195 ± 43 [a,b] | 146 ± 48 | 151 ± 45 |
| Sensorimotor | 194 ± 45 | 150 ± 49 | 159 ± 47 |
| Inferior parietal | 223 ± 55 [a,d] | 147 ± 61 | 139 ± 58 |
| Superior temporal | 197 ± 48 [a,b] | 139 ± 52 | 145 ± 48 |
| Middle and inferior temporal | 207 ± 47 [c,d] | 137 ± 52 | 140 ± 49 |
| Precuneus | 203 ± 52 [d] | 148 ± 57 | 133 ± 55 |
| Anterior cingulate | 158 ± 39 | 123 ± 42 | 138 ± 40 |
| Posterior cingulate | 175 ± 44 [b] | 131 ± 49 | 128 ± 46 |
| Occipital | 206 ± 48 [a,b] | 149 ± 53 | 158 ± 50 |
| Hippocampus | 123 ± 35 [b] | 101 ± 38 | 85 ± 36 |
| Entorhinal | 234 ± 86 [b] | 151 ± 94 | 147 ± 89 |
| Parahippocampal | 142 ± 41 | 102 ± 44 | 111 ± 42 |
| Thalamus | 125 ± 30 | 102 ± 33 | 105 ± 31 |
| Striatum | 100 ± 24 | 86 ± 26 | 90 ± 25 |
| Cerebellum | 121 ± 26 | 99 ± 29 | 104 ± 27 |
| White matter | 83 ± 19 | 70 ± 21 | 75 ± 20 |

[a]$P < 0.05$ versus MCI; [b]$P < 0.05$ versus healthy control subjects; [c]$P < 0.005$ versus MCI; [d]$P < 0.005$ versus healthy control subjects. Values adjusted for genotype, age, and education. Data given as mean ± SD.

seen between patients with MCI and control subjects in any region.

Without partial volume correction, patients with Alzheimer's disease had greater $^{11}$C-PBR28 binding than both patients with MCI and control subjects in middle and inferior temporal cortex, and greater $^{11}$C-PBR28 binding than healthy control subjects only in inferior parietal cortex and entorhinal cortex ($P < 0.05$, Supplementary Table 1 and Supplementary Fig. 1).

When stratified by genotype, high affinity patients with Alzheimer's disease had greater $^{11}$C-PBR28 binding in inferior parietal cortex than high affinity patients with MCI ($P = 0.016$) and high affinity control subjects ($P = 0.024$, Supplementary Fig. 2). Among mixed-affinity subjects, patients with Alzheimer's disease had greater binding in these regions than controls ($P = 0.045$). Greater $^{11}$C-PBR28 binding in mixed-affinity patients with Alzheimer's disease than mixed-affinity patients with MCI was seen at the trend level only ($P = 0.075$). $^{11}$C-PBR28 binding was

the same between patients with MCI and control subjects for both high and mixed-affinity subjects ($P = 1.0$). For cerebellum, no difference was seen between any two diagnostic groups, regardless of genotype ($P > 0.39$).

We next looked for correlations between $^{11}$C-PBR28 binding and performance on selected neuropsychological tests. With partial volume correction—after adjusting for *TSPO* genotype, age, and education—patients with Alzheimer's disease and patients with MCI showed a significant correlation between $^{11}$C-PBR28 binding and impaired performance on Folstein Mini-Mental State Examination, Clinical Dementia Rating Scale Sum of Boxes, Logical Memory Immediate, Block Design, and Trail Making part B tasks (Table 3). The strongest correlations were between $^{11}$C-PBR28 binding and Clinical Dementia Rating Scale score ($r = 0.570$, $P = 0.001$) and performance on Block Design ($r = -0.541$, $P = 0.006$) in inferior parietal lobule. Without partial volume correction, correlations were still seen between $^{11}$C-PBR28 binding

**Table 3** Correlation coefficients (r) between [$^{11}$C]PBR28 binding and performance on neuropsychological testing, adjusted for TSPO genotype, age, and education

| | MMSE | CDR-SB | LM-I | Block Design | Trails B | WCST |
|---|---|---|---|---|---|---|
| Region | | | | | | |
| Prefrontal | −0.379* | 0.429* | −0.432* | −0.360 | 0.323 | 0.127 |
| Inferior parietal | −0.468* | 0.570** | −0.506** | −0.541** | 0.523** | 0.175 |
| Middle and inferior temporal | −0.459* | 0.544** | −0.457* | −0.252 | 0.275 | 0.042 |
| Precuneus | −0.496** | 0.544** | −0.437* | −0.477* | 0.424* | 0.231 |
| Occipital | −0.347 | 0.367 | −0.388* | −0.437* | 0.416* | 0.198 |
| Entorhinal | −0.348 | 0.312 | −0.425* | −0.180 | 0.135 | −0.271 |

*$P < 0.05$, **$P < 0.01$; MMSE = Mini-Mental State Examination; CDR-SB = Clinical Dementia Rating Scale Sum of Boxes; LM-I = Logical Memory Immediate from Wechsler Memory Scale Third Edition; Trails B = Trail Making part B; WCST = Wisconsin Card Sort Test total errors.
On Clinical Dementia Rating Scale Sum of Boxes, Trail Making part B and Wisconsin Card Sort Test, higher score denotes worse performance.

and Clinical Dementia Rating Scale score in inferior parietal lobule, middle and inferior temporal, and entorhinal cortex, and Logical Memory Immediate in entorhinal cortex ($P < 0.05$, Supplementary Table 2). No correlation was seen between $^{11}$C-PBR28 binding and performance on the Wisconsin Card Sort Test Total Errors in any region with or without partial volume correction.

# $^{11}$C-PBR28 binding and grey matter volume

To determine the relationship between neuroinflammation and neurodegeneration in Alzheimer's disease, we looked for correlations between $^{11}$C-PBR28 and grey matter volume in each brain region. With partial volume correction—after adjusting for TSPO genotype, age and education—patients with Alzheimer's disease and patients with MCI showed a significant inverse correlation between $^{11}$C-PBR28 binding and grey matter volume in inferior parietal lobule, superior temporal cortex, middle and inferior temporal cortex, entorhinal cortex, posterior cingulate cortex, parahippocampal gyrus, occipital cortex, precuneus, and cerebellum ($P < 0.05$, Table 4). Notably, no significant correlation was seen between $^{11}$C-PBR28 binding and hippocampal volume ($r = −0.336$, $P = 0.078$).

Without partial volume correction, significant correlation between $^{11}$C-PBR28 and grey matter volume was seen only in inferior parietal lobule ($r = −0.379$, $P = 0.043$) and entorhinal cortex ($r = −0.419$, $P = 0.024$, Supplementary Table 3).

# $^{11}$C-PBR28 binding and amyloid burden

To determine the relationship between neuroinflammation and amyloid burden in Alzheimer's disease, we looked for correlations between $^{11}$C-PBR28 and PIB binding in each brain region. With partial volume correction—after adjusting for TSPO genotype, age, and education—patients with Alzheimer's disease and patients with MCI showed a significant correlation between $^{11}$C-PBR28 and PIB binding in inferior parietal lobule ($r = 0.436$, $P = 0.018$), superior temporal cortex ($r = 0.390$, $P = 0.036$), precuneus ($r = 0.386$, $P = 0.039$), hippocampus ($r = 0.457$, $P = 0.013$), and parahippocampal gyrus ($r = 0.487$, $P = 0.007$). However, without partial volume correction, $^{11}$C-PBR28 binding did not correlate with PIB binding in any brain region.

**Table 4** Correlation between $^{11}$C-PBR28 binding and grey matter voxel count, adjusted for TSPO genotype, age and education

| Region | Correlation coefficient (r) | P-value |
|---|---|---|
| Inferior parietal | −0.557 | 0.002 |
| Superior temporal | −0.462 | 0.012 |
| Middle and inferior temporal | −0.450 | 0.014 |
| Posterior cingulate | −0.420 | 0.023 |
| Entorhinal | −0.410 | 0.027 |
| Precuneus | −0.401 | 0.031 |
| Parahippocampal | −0.396 | 0.033 |
| Occipital | −0.378 | 0.043 |
| Cerebellum | −0.370 | 0.048 |
| Anterior cingulate | −0.337 | 0.074 |
| Hippocampus | −0.332 | 0.078 |
| Sensorimotor | −0.327 | 0.084 |
| Striatum | −0.245 | 0.201 |
| Prefrontal | −0.216 | 0.261 |
| Thalamus | 0.005 | 0.980 |

# $^{11}$C-PBR28 binding and age of onset

To determine if early onset of Alzheimer's disease was associated with greater neuroinflammation, $^{11}$C-PBR28 binding was compared between early-onset (before age 65) and late-onset patients. $^{11}$C-PBR28 image data from patients with Alzheimer's disease and patients with MCI were combined for this analysis. Patients with early-onset had greater binding than late-onset patients, even after correcting for genotype, Mini-Mental State Examination score, and symptom duration. Using the partial volume corrected images $^{11}$C-PBR28 binding was greater in early-onset patients in prefrontal cortex, inferior parietal lobule, precuneus, occipital cortex and striatum ($P < 0.05$, Fig. 2A). Without partial volume correction, early-onset patients had greater $^{11}$C-PBR28 binding in prefrontal cortex, inferior parietal lobule, superior temporal cortex, middle and inferior temporal cortex, occipital cortex, hippocampus and striatum ($P < 0.05$).

Using the partial volume corrected images, $^{11}$C-PBR28 binding—adjusted for genotype, Mini-Mental State Examination
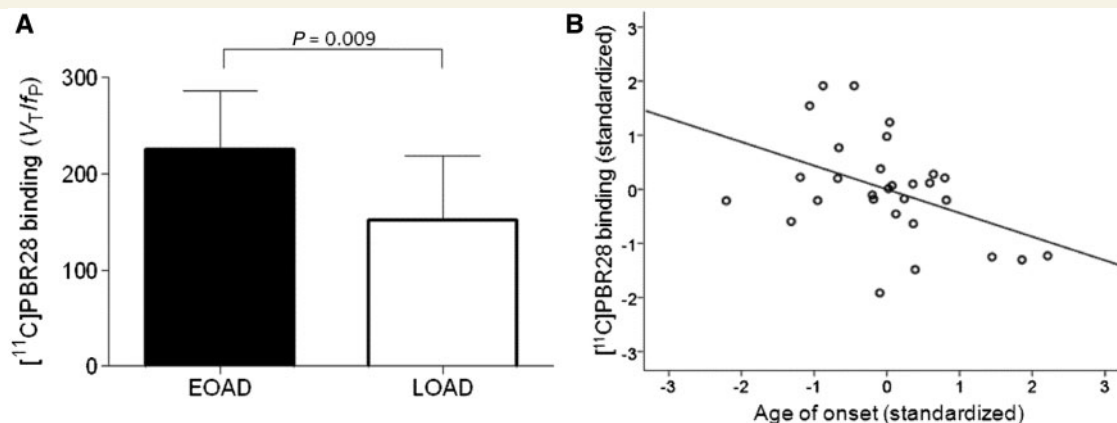
**Figure 2** ^{11}C-PBR28 binding was related to early age of onset in Alzheimer's disease (AD). (**A**) Early-onset (EOAD) patients had greater binding than late-onset patients (LOAD). Bar graphs show values for ^{11}C-PBR28 binding ($V_T / f_P$) in inferior parietal lobule, corrected for partial volume effect. ^{11}C-PBR28 binding values were adjusted for TSPO genotype, Mini-Mental State Examination score, and duration of symptoms. Error bars denote SD. (**B**) ^{11}C-PBR28 binding negatively correlated with age of symptom onset in patients with Alzheimer's disease and MCI. ^{11}C-PBR28 binding values from inferior parietal lobule, corrected for partial volume effect, and age of onset were adjusted for *TSPO* genotype, Mini-Mental State Examination score, and duration of symptoms before correlative analysis. Standardized adjusted values are shown. Correlation coefficient (r) = $-0.438$, $P = 0.017$.

**Table 5** Correlation between ^{11}C-PBR28 binding and age of symptom onset, adjusted for genotype, Mini-Mental State Examination score and duration of symptoms

| Region | Correlation coefficient (r) | P-value |
|---|---|---|
| Inferior parietal | $-0.438$ | 0.017 |
| Striatum | $-0.412$ | 0.027 |
| Precuneus | $-0.402$ | 0.031 |
| Prefrontal | $-0.335$ | 0.076 |
| Occipital | $-0.320$ | 0.090 |
| Thalamus | $-0.318$ | 0.093 |
| Sensorimotor | $-0.291$ | 0.125 |
| Cerebellum | $-0.286$ | 0.133 |
| Posterior cingulate | $-0.267$ | 0.161 |
| Parahippocampal | $-0.251$ | 0.189 |
| Middle and inferior temporal | $-0.250$ | 0.192 |
| Superior temporal | $-0.250$ | 0.192 |
| Anterior cingulate | $-0.246$ | 0.198 |
| Hippocampus | $-0.227$ | 0.235 |
| Entorhinal | $-0.111$ | 0.566 |

score and symptom duration negatively correlated with age of onset in inferior parietal lobule, precuneus and striatum ($P < 0.035$, Fig. 2B, Table 5). Without atrophy correction, ^{11}C-PBR28 binding negatively correlated with age of onset in these same regions and in occipital cortex, hippocampus, and thalamus ($P < 0.05$, Supplementary Table 4).

# Discussion

We found that Alzheimer's disease, but not MCI, is associated with increased ^{11}C-PBR28 binding in cortical regions typically affected by the disease, despite the fact that patients with MCI had

amyloid pathology and hippocampal atrophy as assessed by PIB PET and MRI volumetric analysis. In addition, ^{11}C-PBR28 binding correlates with clinical severity and reduced grey matter volume in several brain regions, most notably the temporo-parietal regions with highest TSPO density. Finally, early-onset patients have greater ^{11}C-PBR28 binding than late-onset patients, and earlier age of onset is associated with increased ^{11}C-PBR28 binding, particularly in parietal cortex. Collectively, these results suggest that increased TSPO expression by activated microglia, measureable by ^{11}C-PBR28, occurs after the clinical conversion of MCI to Alzheimer's disease and continues to increase as the disease progresses. These changes appear to be amplified in patients who develop disease symptoms at an early age.

In our study, ^{11}C-PBR28 did not detect microglial activation in subjects with MCI. Most pathological studies and some PET studies have shown results that strongly suggest neuroinflammatory changes occur in both patients with MCI and patients with Alzheimer's disease (Cagnin *et al.*, 2001; Edison *et al.*, 2008; Okello *et al.*, 2009a; Eikelenboom *et al.*, 2010). Therefore, ^{11}C-PBR28 may not be sensitive enough to detect increased TSPO density in patients with MCI, even when only high affinity subjects are included. We speculate that ^{11}C-PBR28 is able to detect increases in TSPO density beyond what is seen in patients with MCI, and therefore ^{11}C-PBR28 binding has promise as an objective measurement of conversion from MCI to dementia caused by Alzheimer's disease. However, longitudinal study is needed to investigate this hypothesis.

In addition, this study showed that early-onset patients have greater ^{11}C-PBR28 binding than late-onset patients. Previous studies have shown worsening atrophy and glucose metabolism in early-onset patients compared with late-onset patients at similar clinical stage (Frisoni *et al.*, 2005, 2007; Kim *et al.*, 2005). However, PIB binding was found to be similar between age-of-onset groups (Rabinovici *et al.*, 2010). In our study, greater ^{11}C-PBR28 binding was seen in frontal and parietal regions,

echoing studies that found greater fronto-parietal atrophy and dysfunction in patients with early-onset Alzheimer's disease (Suribhatla et al., 2004; Shiino et al., 2006; Karas et al., 2007; Licht et al., 2007). Thus, instead of amyloid burden, microglial activation might be the driving pathogenic factor in the more precipitous decline, and may explain the more severe executive and visuospatial impairment in younger patients.

Notably, this study was the first to implement TSPO genotype correction to improve data interpretation in a clinical study using a second generation TSPO radioligand. Our previous in vitro study using ^{3}H-PBR28 showed that genotype correction improved detection of differences in TSPO density in post-mortem brain tissue from patients with schizophrenia compared with control subjects (Kreisl et al., 2013). Genotype correction reduces variance in PET data caused by differential affinity, thereby increasing statistical power. In addition, genotype correction decreases type 1 or type 2 errors due to unequal inclusion of mixed-affinity subjects in patient and control groups. A previous study that used the second generation radioligand ^{11}C-DAA1106 detected differences between Alzheimer's disease and controls, though it was published before the discovery of differential affinity in this radioligand (Yasuno et al., 2008). However, the rs6971 polymorphism is rare in the Japanese population (~4% allelic frequency) and unlikely to have affected the results in that study (http://hapmap.ncbi.nlm.nih.gov/cgi-perl/snp_details_phase3?name=rs6971&source=hapmap-p28_B36&tmpl=snp_details_phase3). Different results might have been obtained if that study had included participants of Caucasian or African-American ancestry, in whom the rs6971 polymorphism has an allelic frequency of ~30%.

Previous studies using [11]C-(R)-PK 11195 showed conflicting results regarding whether or not TSPO density is increased in MCI or Alzheimer's disease (Cagnin et al., 2001; Edison et al., 2008; Okello et al., 2009a; Wiley et al., 2009; Schuitemaker et al., 2013) and whether or not TSPO binding correlates with clinical severity in Alzheimer's disease (Edison et al., 2008; Schuitemaker et al., 2013). However, the one [11]C-(R)-PK 11195 study that showed a correlation between TSPO binding and cognitive impairment also used PIB imaging to measure amyloid plaque deposition (Edison et al., 2008). In that study, similar to ours, all patients had PIB binding greater than control subjects, strongly suggesting that patients with non-Alzheimer's disease pathology and controls with incidental Alzheimer's disease pathology were excluded. Our results therefore confirm that TSPO binding is elevated in dementia patients with evidence of amyloid pathology on PET imaging.

Even with correction for genotype, PET imaging with ^{11}C-PBR28 has several limitations. First, low affinity subjects, who have negligible binding to PBR28, had to be excluded from the study. Second, while adjusting $V_T / f_P$ values for genotype corrects for the lower binding caused by the mixed-affinity genotype, the fact remains that mixed-affinity subjects have a lower ratio of specific-to-non-specific binding than high affinity subjects. Therefore, ^{11}C-PBR28 PET imaging of mixed-affinity subjects likely has reduced sensitivity to detect differences in TSPO density than imaging only high affinity subjects. Third, PBR28 binds to TSPO, which is expressed by astrocytes as well as microglia. Therefore, increased TSPO density could reflect acute injury with associated activation of microglia, or alternatively could

represent past damage with residual astrocytosis, such as that seen in chronic epilepsy (Librizzi et al., 2012). Increased ^{11}C-PBR28 binding in Alzheimer's disease therefore does not necessarily reflect ongoing activation of microglia. However, results from transgenic mouse and autopsy studies have shown that increased TSPO density in Alzheimer's disease brain co-localizes to microglia rather than astrocytes (Venneti et al., 2008; Gulyas et al., 2009). Finally, even after genotype correction, variance in ^{11}C-PBR28 binding remains, so that overlap exists between Alzheimer's disease, MCI, and control values. Whereas age, education, gender, and non-steroidal anti-inflammatory drug and cholinesterase use did not appear to influence ^{11}C-PBR28 binding, other yet-to-be-determined factors besides genotype may affect ^{11}C-PBR28 binding within any diagnostic group. Identifying such factors is expected to further reduce variance and improve the ability of ^{11}C-PBR28 to detect differences in TSPO density in Alzheimer's disease and other diseases associated with inflammation.

Like many other PET studies of disorders with brain atrophy, this paper partially compensated for atrophy with partial volume correction. Although partial volume correction is intended to compensate and correct for atrophy, it can theoretically induce positive results when none actually exists. To minimize false positive results, we regard as truly significant only those which are so both with and without partial volume correction. For example, with regard to the primary result of this paper, the elevation of TSPO binding in Alzheimer's disease compared with control subjects and MCI was statistically significant in at least some regions both with and without partial volume correction. However, with regard to the secondary results of this paper, only three of the four correlations to TSPO binding were significant both with and without partial volume correction. That is, the correlation with TSPO binding was dually significant for neuropsychological measures, grey matter volume, and age of onset but not for amyloid load. Thus, we are not as confident in the true correlation of TSPO and amyloid load because it was statistically significant only after partial volume correction. Furthermore, among these four variables, only amyloid load was itself measured with partial volume correction, consistent with several other studies using PIB (Price et al., 2005; Landau et al., 2013). Thus, the cause of the potentially false positive correlation may be a co-linear effect induced by multiplying both variables (TSPO binding and amyloid load) by the same scaling factor generated by partial volume correction. Finally, in contrast to TSPO binding, amyloid load does not correlate well with clinical severity (Edison et al., 2008) and shows little to no increase after conversion to dementia (Scheinin et al., 2009; Villemagne et al., 2011; Villain et al., 2012). TSPO binding may therefore provide complementary information to amyloid load regarding disease pathology and may be a more dynamic marker of disease progression.

# Conclusion

Alzheimer's disease, but not MCI, is associated with increased TSPO expression as measured with ^{11}C-PBR28 PET, mostly in temporal and parietal regions known to be affected by amyloid plaque pathology. In these same regions, TSPO correlates with clinical

severity and grey matter loss, but less clearly with fibrillar amyloid burden. Early-onset patients have greater frontal and parietal TSPO binding than late-onset patients, which might explain the more precipitous disease course in patients who develop Alzheimer's disease at an early age, and the prevalence of frontoparietal dysfunction in early-onset patients. *In vivo* measurement of TSPO expression has promise in longitudinal studies to detect disease progression from MCI to Alzheimer's disease, and a radioligand with even greater sensitivity than ^{11}C-PBR28, which does not distinguish different affinity states of TSPO, would be advantageous.

# Acknowledgements

# Funding

# Supplementary material

Supplementary material is available at *Brain* online.

# References

Abi-Dargham A, Gandelman M, Zoghbi SS, Laruelle M, Baldwin RM, Randall P, et al. Reproducibility of SPECT measurement of benzodiazepine receptors in human brain with iodine-123-iomazenil. J Nucl Med 1995; 36: 167–75.

Albert MS, DeKosky ST, Dickson D, Dubois B, Feldman HH, Fox NC, et al. The diagnosis of mild cognitive impairment due to Alzheimer's disease: recommendations from the National Institute on Aging-Alzheimer's Association workgroups on diagnostic guidelines for Alzheimer's disease. Alzheimers Dement 2011; 7: 270–9.

Cagnin A, Brooks DJ, Kennedy AM, Gunn RN, Myers R, Turkheimer FE, et al. In-vivo measurement of activated microglia in dementia. Lancet 2001; 358: 461–7.

Chauveau F, Boutin H, Van Camp N, Dolle F, Tavitian B. Nuclear imaging of neuroinflammation: a comprehensive review of [11C]PK11195 challengers. Eur J Nucl Med Mol Imaging 2008; 35: 2304–19.

Craft JM, Watterson DM, Van Eldik LJ. Human amyloid beta-induced neuroinflammation is an early event in neurodegeneration. Glia 2006; 53: 484–90.

Desikan RS, Segonne F, Fischl B, Quinn BT, Dickerson BC, Blacker D, et al. An automated labeling system for subdividing the human cerebral cortex on MRI scans into gyral based regions of interest. Neuroimage 2006; 31: 968–80.

Edison P, Archer HA, Gerhard A, Hinz R, Pavese N, Turkheimer FE, et al. Microglia, amyloid, and cognition in Alzheimer's disease: an [11C](R)PK11195-PET and [11C]PIB-PET study. Neurobiol Dis 2008; 32: 412–9.

Eikelenboom P, van Exel E, Hoozemans JJ, Veerhuis R, Rozemuller AJ, van Gool WA. Neuroinflammation - an early event in both the history and pathogenesis of Alzheimer's disease. Neurodegener Dis 2010; 7: 38–41.

El Khoury J, Toft M, Hickman SE, Means TK, Terada K, Geula C, et al. Ccr2 deficiency impairs microglial accumulation and accelerates progression of Alzheimer-like disease. Nat Med 2007; 13: 432–8.

Fischl B, Salat DH, Busa E, Albert M, Dieterich M, Haselgrove C, et al. Whole brain segmentation: automated labeling of neuroanatomical structures in the human brain. Neuron 2002; 33: 341–55.

Fischl B, van der Kouwe A, Destrieux C, Halgren E, Segonne F, Salat DH, et al. Automatically parcellating the human cerebral cortex. Cereb Cortex 2004; 14: 11–22.

Frisoni GB, Pievani M, Testa C, Sabattoli F, Bresciani L, Bonetti M, et al. The topography of grey matter involvement in early and late onset Alzheimer's disease. Brain 2007; 130: 720–30.

Frisoni GB, Testa C, Sabattoli F, Beltramello A, Soininen H, Laakso MP. Structural correlates of early and late onset Alzheimer's disease: voxel based morphometry study. J Neurol Neurosurg Psychiatry 2005; 76: 112–4.

Fujita M, Imaizumi M, Zoghbi SS, Fujimura Y, Farris AG, Suhara T, et al. Kinetic analysis in healthy humans of a novel positron emission tomography radioligand to image the peripheral benzodiazepine receptor, a potential biomarker for inflammation. Neuroimage 2008; 40: 43–52.

Gulyas B, Makkai B, Kasa P, Gulya K, Bakota L, Varszegi S, et al. A comparative autoradiography study in post mortem whole hemisphere human brain slices taken from Alzheimer patients and age-matched controls using two radiolabelled DAA1106 analogues with high affinity to the peripheral benzodiazepine receptor (PBR) system. Neurochem Int 2009; 54: 28–36.

Ikoma Y, Yasuno F, Ito H, Suhara T, Ota M, Toyama H, et al. Quantitative analysis for estimating binding potential of the peripheral benzodiazepine receptor with [(11)C]DAA1106. J Cereb Blood Flow Metab 2007; 27: 173–84.

Imaizumi M, Briard E, Zoghbi SS, Gourley JP, Hong J, Musachio JL, et al. Kinetic evaluation in nonhuman primates of two new PET ligands for peripheral benzodiazepine receptors in brain. Synapse 2007; 61: 595–605.

Innis RB, Cunningham VJ, Delforge J, Fujita M, Gjedde A, Gunn RN, et al. Consensus nomenclature for in vivo imaging of reversibly binding radioligands. J Cereb Blood Flow Metab 2007; 27: 1533–9.

Jack CR Jr, Lowe VJ, Senjem ML, Weigand SD, Kemp BJ, Shiung MM, et al. 11C PiB and structural MRI provide complementary information

in imaging of Alzheimer's disease and amnestic mild cognitive impairment. Brain 2008; 131: 665–80.

Karas G, Scheltens P, Rombouts S, van Schijndel R, Klein M, Jones B, et al. Precuneus atrophy in early-onset Alzheimer's disease: a morphometric structural MRI study. Neuroradiology 2007; 49: 967–76.

Kim EJ, Cho SS, Jeong Y, Park KC, Kang SJ, Kang E, et al. Glucose metabolism in early onset versus late onset Alzheimer's disease: an SPM analysis of 120 patients. Brain 2005; 128: 1790–801.

Klunk WE, Engler H, Nordberg A, Wang Y, Blomqvist G, Holt DP, et al. Imaging brain amyloid in Alzheimer's disease with Pittsburgh Compound-B. Ann Neurol 2004; 55: 306–19.

Kreisl WC, Fujita M, Fujimura Y, Kimura N, Jenko KJ, Kannan P, et al. Comparison of [(11)C]-(R)-PK 11195 and [(11)C]PBR28, two radioligands for translocator protein (18 kDa) in human and monkey: implications for positron emission tomographic imaging of this inflammation biomarker. Neuroimage 2010; 49: 2924–32.

Kreisl WC, Jenko KJ, Hines CS, Hyoung Lyoo C, Corona W, Morse CL, et al. A genetic polymorphism for translocator protein 18 kDa affects both *in vitro* and *in vivo* radioligand binding in human brain to this putative biomarker of neuroinflammation. J Cereb Blood Flow Metab 2013; 33: 53–8.

Landau SM, Breault C, Joshi AD, Pontecorvo M, Mathis CA, Jagust WJ, et al. Amyloid-beta imaging with Pittsburgh compound B and florbetapir: comparing radiotracers and quantification methods. J Nucl Med 2013; 54: 70–7.

Librizzi L, Noe F, Vezzani A, de Curtis M, Ravizza T. Seizure-induced brain-borne inflammation sustains seizure recurrence and blood-brain barrier damage. Ann Neurol 2012; 72: 82–90.

Licht EA, McMurtray AM, Saul RE, Mendez MF. Cognitive differences between early- and late-onset Alzheimer's disease. Am J Alzheimers Dis Other Demen 2007; 22: 218–22.

McGeer EG, McGeer PL. Inflammatory processes in Alzheimer's disease. Prog Neuropsychopharmacol Biol Psychiatry 2003; 27: 741–9.

McKhann G, Drachman D, Folstein M, Katzman R, Price D, Stadlan EM. Clinical diagnosis of Alzheimer's disease: report of the NINCDS-ADRDA Work Group under the auspices of Department of Health and Human Services Task Force on Alzheimer's Disease. Neurology 1984; 34: 939–44.

McKhann GM, Knopman DS, Chertkow H, Hyman BT, Jack CR Jr, Kawas CH, et al. The diagnosis of dementia due to Alzheimer's disease: recommendations from the National Institute on Aging-Alzheimer's Association workgroups on diagnostic guidelines for Alzheimer's disease. Alzheimers Dement 2011; 7: 263–9.

Okello A, Edison P, Archer HA, Turkheimer FE, Kennedy J, Bullock R, et al. Microglial activation and amyloid deposition in mild cognitive impairment: a PET study. Neurology 2009a; 72: 56–62.

Okello A, Koivunen J, Edison P, Archer HA, Turkheimer FE, Nagren K, et al. Conversion of amyloid positive and negative MCI to AD over 3 years: an 11C-PIB PET study. Neurology 2009b; 73: 754–60.

Owen DR, Gunn RN, Rabiner EA, Bennacef I, Fujita M, Kreisl WC, et al. Mixed-affinity binding in humans with 18-kDa translocator protein ligands. J Nucl Med 2011; 52: 24–32.

Owen DR, Yeo AJ, Gunn RN, Song K, Wadsworth G, Lewis A, et al. An 18-kDa translocator protein (TSPO) polymorphism explains differences in binding affinity of the PET radioligand PBR28. J Cereb Blood Flow Metab 2012; 32: 1–5.

Papadopoulos V, Baraldi M, Guilarte TR, Knudsen TB, Lacapere JJ, Lindemann P, et al. Translocator protein (18kDa): new nomenclature for the peripheral-type benzodiazepine receptor based on its structure and molecular function. Trends Pharmacol Sci 2006; 27: 402–9.

Petersen RC. Mild cognitive impairment as a diagnostic entity. J Intern Med 2004; 256: 183–94.

Petrou M, Bohnen NI, Muller ML, Koeppe RA, Albin RL, Frey KA. Abeta-amyloid deposition in patients with Parkinson disease at risk for development of dementia. Neurology 2012; 79: 1161–7.

Price JC, Klunk WE, Lopresti BJ, Lu X, Hoge JA, Ziolko SK, et al. Kinetic modeling of amyloid binding in humans using PET imaging and Pittsburgh Compound-B. J Cereb Blood Flow Metab 2005; 25: 1528–47.

Rabinovici GD, Furst AJ, Alkalay A, Racine CA, O'Neil JP, Janabi M, et al. Increased metabolic vulnerability in early-onset Alzheimer's disease is not related to amyloid burden. Brain 2010; 133: 512–28.

Scheinin NM, Aalto S, Koikkalainen J, Lotjonen J, Karrasch M, Kemppainen N, et al. Follow-up of [11C]PIB uptake and brain volume in patients with Alzheimer disease and controls. Neurology 2009; 73: 1186–92.

Schuitemaker A, Kropholler MA, Boellaard R, van der Flier WM, Kloet RW, van der Doef TF, et al. Microglial activation in Alzheimer's disease: an (R)-[(11)C]PK11195 positron emission tomography study. Neurobiol Aging 2013; 34: 128–36.

Shiino A, Watanabe T, Maeda K, Kotani E, Akiguchi I, Matsuda M. Four subgroups of Alzheimer's disease based on patterns of atrophy using VBM and a unique pattern for early onset disease. Neuroimage 2006; 33: 17–26.

Streit WJ, Braak H, Xue QS, Bechmann I. Dystrophic (senescent) rather than activated microglial cells are associated with tau pathology and likely precede neurodegeneration in Alzheimer's disease. Acta Neuropathol 2009; 118: 475–85.

Suribhatla S, Baillon S, Dennis M, Marudkar M, Muhammad S, Munro D, et al. Neuropsychological performance in early and late onset Alzheimer's disease: comparisons in a memory clinic population. Int J Geriatr Psychiatry 2004; 19: 1140–7.

Thomas BA, Erlandsson K, Modat M, Thurfjell L, Vandenberghe R, Ourselin S, et al. The importance of appropriate partial volume correction for PET quantification in Alzheimer's disease. Eur J Nucl Med Mol Imaging 2011; 38: 1104–19.

Venneti S, Wang G, Nguyen J, Wiley CA. The positron emission tomography ligand DAA1106 binds with high affinity to activated microglia in human neurological disorders. J Neuropathol Exp Neurol 2008; 67: 1001–10.

Villain N, Chetelat G, Grassiot B, Bourgeat P, Jones G, Ellis KA, et al. Regional dynamics of amyloid-beta deposition in healthy elderly, mild cognitive impairment and Alzheimer's disease: a voxelwise PiB-PET longitudinal study. Brain 2012; 135: 2126–39.

Villemagne VL, Pike KE, Chetelat G, Ellis KA, Mulligan RS, Bourgeat P, et al. Longitudinal assessment of Abeta and cognition in aging and Alzheimer disease. Ann Neurol 2011; 69: 181–92.

Weintraub S, Salmon D, Mercaldo N, Ferris S, Graff-Radford NR, Chui H, et al. The Alzheimer's Disease Centers' Uniform Data Set (UDS): the neuropsychologic test battery. Alzheimer Dis Assoc Disord 2009; 23: 91–101.

Wiley CA, Lopresti BJ, Venneti S, Price J, Klunk WE, DeKosky ST, et al. Carbon 11-labeled Pittsburgh compound B and carbon 11-labeled (R)-PK11195 positron emission tomographic imaging in Alzheimer disease. Arch Neurol 2009; 66: 60–7.

Wolk DA, Price JC, Saxton JA, Snitz BE, James JA, Lopez OL, et al. Amyloid imaging in mild cognitive impairment subtypes. Ann Neurol 2009; 65: 557–68.

Xiang Z, Haroutunian V, Ho L, Purohit D, Pasinetti GM. Microglia activation in the brain as inflammatory biomarker of Alzheimer's disease neuropathology and clinical dementia. Dis Markers 2006; 22: 95–102.

Yasuno F, Ota M, Kosaka J, Ito H, Higuchi M, Doronbekov TK, et al. Increased binding of peripheral benzodiazepine receptor in Alzheimer's disease measured by positron emission tomography with [11C]DAA1106. Biol Psychiatry 2008; 64: 835–41.

Zoghbi SS, Shetty HU, Ichise M, Fujita M, Imaizumi M, Liow JS, et al. PET imaging of the dopamine transporter with 18F-FECNT: a polar radiometabolite confounds brain radioligand measurements. J Nucl Med 2006; 47: 520–7.